JOURNAL OF THE MECHANICAL BEHAVIOR OF BIOMEDICAL MATERIALS 27 (2013) 19–32

Available online at www.sciencedirect.com

ScienceDirect

www.elsevier.com/locate/jmbbm

Research Paper

Rotary-bending fatigue characteristics of medical-grade Nitinol wire

A.R. Pelton[a,*], J. Fino-Decker[a], L. Vien[a], C. Bonsignore[a], P. Saffari[a], M. Launey[a], M.R. Mitchell[b]

[a]Nitinol Devices and Components, Inc. 47533 Westinghouse Dr., Fremont, CA 94539, USA
[b]Mechanics and Materials Consulting, LLC 4447 Acrete Lane, Flagstaff, AZ 86004, USA

ARTICLE INFO

Article history:
Received 9 May 2013
Received in revised form
30 May 2013
Accepted 6 June 2013
Available online 27 June 2013

Keywords:
Nitinol
Fatigue
Shape memory
Pseudoelasticity
Strain amplitude

ABSTRACT

The rotary bending fatigue properties of medical-grade Nitinol wires were investigated under conditions of 0.5–10% strain amplitudes to a maximum of 10^7 cycles. The results from this study provide insight into the behavior of Nitinol under fully reversed ($\varepsilon_{min}/\varepsilon_{max}=-1$) fatigue conditions for three compositions, two surface conditions and three test temperatures. For pseudoelastic conditions there are four distinct regions of the strain-cycle curves that are related to phases (austenite, stress-induced martensite, and R-Phase) and their respective strain accommodation mechanisms. In contrast, there are only two regions for the strain-cycle curves for thermal martensite. It was further observed that the strain amplitude to achieve 10^7-cycles increases with both decreasing test temperature and increasing transformation temperature. Fatigue behavior was not, however, strongly influenced by wire surface condition. SEM of the fracture surfaces showed that the fatigue fracture area increased with decreasing strain amplitude. Finite element analysis was used to illustrate strain distributions across the wire as well as to calculate the tension-compression contributions to the rotary bending curves. The results from this investigation are discussed with respect to mechanisms of strain accommodation under cyclic tensile and compressive conditions.

1. Introduction

Nitinol (NiTi) exhibits well-known shape memory and pseudoelastic effects that are due to a first-order cubic (B2) to monoclinic (B19') martensitic transformation (Bhattacharya, 2003; Otsuka and Ren, 2005). This temperature- or stress-induced transformation is fully reversible, whereby strains as great as 10% may be fully recovered. Consequently, Nitinol has become the material of choice for many medical devices that undergo repetitive strain excursions, such as self-expanding, endovascular stents (Duerig and Pelton, 1999; Stöckel and Pelton, 2004) and endodontic dental files (Thompson, 2000; Bahia and Martins, 2005; Young and Van Vliet, 2005). Self-expanding Nitinol stents are initially strained 6–10% during crimping, and insertion into a catheter delivery system, with a partial strain release with deployment into the diseased vessel.

*Corresponding author. Tel.: +1 510 683 2037; fax: 1 510 683 2001.
E-mail addresses: alan.pelton@nitinol.com (A.R. Pelton), lot.vien@nitinol.com (L. Vien), jennifer.decker@nitinol.com (J. Fino-Decker), lot.vien@nitinol.com (L. Vien), craig.bonsignore@nitinol.com (C. Bonsignore), payman.saffari@nitinol.com (P. Saffari), max.launey@nitinol.com (M. Launey), mrmitchell@illinoisalumni.org (M.R. Mitchell).

1751-6161/$ - see front matter © 2013 Elsevier Ltd. All rights reserved.
http://dx.doi.org/10.1016/j.jmbbm.2013.06.003

The stent is then subjected to multi-axial cyclic deformations with combinations of mean strain (from stent/vessel oversizing) and strain amplitude (from cardiac cycles and musculoskeletal motions) (Pelton and Schroeder, 2008). In contrast, the outer fibers of the endodontic wires are subjected to alternating compressive and tensile strains with a (nominal) net zero-mean strain for many thousands or even millions of cycles.

A recent review article focused on the effects of processing and microstructure on Nitinol fatigue behavior under strain- and stress-life or damage tolerant conditions (Robertson and Pelton, 2012). It is now well known that thermomechanical processing has a profound effect on the mechanical behavior of Nitinol (Pelton and DiCello, 2000; Drexel and Selvadury, 2008; Pelton, 2011). Surprisingly, however, very few rotary-bending fatigue investigations have been published on medical-grade Nitinol with modern thermomechanical processing (Reinoehl et al., 2001; Sawaguchi and Kausträter, 2003; Sheriff and Pelton, 2005; Wick and Gong, 2005; Young and Van Vliet, 2005). Rotary-bending fatigue studies are a convenient method to determine the effects of processing parameters, compositional variations, and surface conditions on fatigue behavior of wire or microtubing under (nominal) zero-mean strain conditions. For these testing conditions, strain amplitude is approximated by the ratio of wire radius to radius of curvature, so a range of strain amplitudes may be achieved with slight adjustments to the bending curvature.

Miyazaki and co-workers studied the effects of strain amplitude (0.8–3.5%) and temperature (35–125 °C) on fatigue life on $Ni_{50.9}Ti_{49.1}$ wires to 10^6 cycles (Kim and Miyazaki, 1997; Miyazaki and Mizukoshi, 1999). Their wires were cold drawn 30% and then aged at 400 °C for 1 h, resulting in an Austenite Finish (A_f) temperature of 40 °C. A general trend of increasing fatigue life with decreasing test temperature in the low-cycle fatigue regions (high and intermediate strain–amplitude regions) was observed. From their limited data, the fatigue strain at 10^6 cycles appeared to be insensitive to temperature to a strain amplitude of 0.8%. The authors characterized the fatigue behavior with respect to the phases present at the respective test temperatures. Reinoehl and Bradley compared fatigue results at room temperature from 0.8% to 2.1% strain amplitude to a maximum of 10^7 cycles for wires that were manufactured from two ingot sources (Reinoehl et al., 2001). The two sets of wires were cold-drawn to a diameter of 0.267 mm and thermally treated at 500 °C to achieve A_f values of ~10 °C. They concluded that there were no substantial differences in the fatigue behavior despite the differences in ingot source and inclusion type, size and distribution. Sawaguchi and Kausträter (2003) measured the number of cycles to failure out to 10^6 cycles with strain amplitudes between 0.75% and 3% with three wire diameters (1.0, 1.2, and 1.4 mm). The $Ni_{50.9}Ti_{49.1}$wires were produced by hot extrusion, followed by 40% cold work, straightened at 510 °C for 1 min with a resultant 50 nm grains and transformation temperatures that ranged from 11 to 26 °C (DSC austenite peak temperature). However, since their experiments were conducted in room temperature air (non-isothermal conditions), they also observed differences with rotation speed as well as wire diameter.

The purpose of our research, therefore, is to report on an investigation of the rotating bending fatigue characteristics of shape memory and pseudoelastic medical-grade Nitinol wires as part of a larger investigation of Nitinol fatigue behavior. Specifically, medical-grade wires with four compositions, two surface conditions, and three test temperatures were investigated from 0.5% to 10% strain amplitudes to 10^7 cycles. These data are compared to conventional fatigue theories and are characterized with finite element analysis and fractography.

Table 1 – Wire materials and testing conditions.

Composition	A_f (°C)	Surface condition
$Ni_{50.8}Ti_{49.2}$	2	Bright
$Ni_{50.8}Ti_{49.2}$	4	Black
$Ni_{50.6}Ti_{49.4}$	7	Black
$Ni_{49.5}Ti_{50.5}$	64	Black

2. Material and methods

2.1. *Material surface and transformation temperature*

Table 1 summarizes the compositions, A_f, and surface conditions of the commercially available binary, 0.6 mm diameter Nitinol wires used in this investigation. Two of the wires have a composition of $Ni_{50.8}Ti_{49.2}$, whereas another wire had a slightly lower Ni concentration ($Ni_{50.6}Ti_{49.4}$) but was processed to achieve similar transformational and mechanical properties; all three wires conform to ASTM F2063 (ASTM, 2005). The fourth wire, $Ni_{49.5}Ti_{50.5}$, has a greater Ti content with a concomitant greater transformation temperature than the other wires. The wires were processed from vacuum arc re-melt (VAR) ingots and were manufactured in-house per industry standard methods (Pelton and DiCello, 2000). Prior to final thermal shape setting at ~500 °C, the wires were drawn with approximately 45% cold work (as measured by cross-sectional area reduction after the previous full anneal). The resultant transformation temperatures were approximately 5 °C (range 2–7 °C) for the nickel-rich compositions and 64 °C for the titanium-rich composition, measured by bend-free recovery methods per ASTM F2082 (ASTM, 2006a).

Surface conditions of the wires were characterized as *black* or *bright*; both conditions are used commercially as starting material for wire-based Nitinol medical devices. The *black* wires have their native thermal oxide with approximately 300 nm thickness. The *bright* wires were mechanically polished continuously after the wire drawing operation to remove the black oxide and draw lines as well as to smooth the surface. The mechanical polish is approximately equivalent to a 400 grit mechanical polish.

2.2. *Uniaxial tensile characterization*

Monotonic uniaxial tensile tests on a minimum of three wires from each condition were conducted with a mechanical

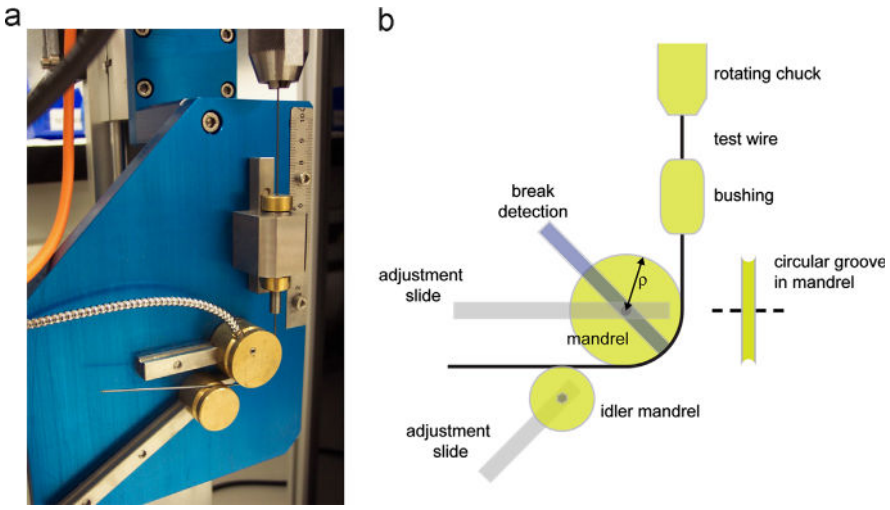

Fig. 1 – (a) Photograph and (b) schematic of the custom-built rotary bend fatigue tester. The environmental-controlled test chamber is not shown. See vertical scale (cm) for relative dimensions.

testing machine (Instron Model 5500R) equipped with an environmental chamber. An extension rate of 0.5 mm/min with an extensometer per guidelines in ASTM F2516 (ASTM, 2006b) was used at test temperatures of –25, 23 and 60 °C.

2.3. *Rotary bending fatigue testing*

Rotary bending tests were performed using a guided rotary bend tester as shown in Fig. 1 that was also used for previous studies (Graham and VanDoren, 2004; Sheriff and Pelton, 2005; Wick and Gong, 2005; Morgan and Wick, 2008). The wire specimens were rotated around a series of fixed diameter mandrels. The mandrels were machined from Delrin® Acetal Resin (DuPont) rods to minimize surface wear on the Nitinol wires.

Strain amplitudes were estimated by:

$$\varepsilon_a = \frac{d}{2\rho} \quad (1)$$

where d is the wire diameter, and ρ is the radius of curvature of the mandrels used. Test temperatures of –25, 23, and 60 °C were obtained with a temperature-control re-circulating unit. Chilled methyl alcohol was used for the lowest test temperature (–25 °C), whereas tests at 23 and 60 °C were performed in distilled water. These temperatures were chosen to provide a wide range of temperatures that bracket relevant medical device applications. Tests were conducted at a maximum rotational speed of 2000 rpm[1] until fracture was detected with the optical fiber, break-detection system. High-cycle fatigue tests were conducted to a maximum of 10^7 cycles. A minimum of five wires per strain level was tested for each condition with 210 mm wire lengths. The wire fracture surfaces were examined with an SEM (JEOL model 5600 or FEI Quanta 200 3D) in both the secondary electron and back-scattered imaging modes.

[1]For comparison, a limited number of tests were conducted at 300 rpm; no discernible differences were observed in the fatigue behavior of the wires.

2.4. *Finite element analysis*

A non-linear Finite Element Analysis (FEA) model of the rotary bending loading was developed to determine local stresses and strains in the Nitinol wire subjected to 360° rotations with different bending radii. The commercial FEA package Abaqus®/Standard version 6.12-1 was used in combination with the user-defined material subroutine (UMAT) for these computational analyses. The non-linear mechanical and thermal input properties for the Nitinol UMAT were derived from the uniaxial tension tests performed on the $Ni_{50.8}Ti_{49.2}$ bright Nitinol wires, per industry practice. Since uniaxial compression testing on such fine wire samples is not possible, the FEA model incorporates the convention of compressive transformation stress equal to 1.5 × the tensile transformation stress (Dessault Systèmes, 1658). Table 2 provides the parameters used for the FEA that were extracted from the uniaxial tensile tests from Fig. 2.

3. Results

3.1. *Uniaxial tensile mechanical properties*

Fig. 2 shows the uniaxial stress–strain properties in tension at –25, 23, and 60 °C of the four wires: (a) $Ni_{50.8}Ti_{49.2}$ bright, (b) $Ni_{50.8}Ti_{49.2}$ black, (c) $Ni_{50.6}Ti_{49.4}$ black, and (d) $Ni_{49.5}Ti_{50.5}$ black. The curves from the Ni-rich compositions show the expected differences in elastic modulus and plateau stress with temperature, whereby both parameters increase with increasing test temperature. The upper plateau stress rate ($d\sigma/dT$) is approximately 5 MPa/°C, comparable to published data from medical-grade Nitinol pseudoelastic wire (Pelton and DiCello et al. 2000). Furthermore, the maximum strain at the end of the stress plateau for the $Ni_{50.8}Ti_{49.2}$ and $Ni_{50.6}Ti_{49.4}$ wires increases with increasing test temperature; for example, the maximum plateau strain at 60 °C is 7.5% compared with 6.3%

at 23 °C for the $Ni_{50.8}Ti_{49.2}$ bright wires. This observation supports the increased stability of austenite with respect to the (stress-induced) martensitic phase transformation at temperatures above A_f. The ultimate tensile stress and total elongation values are comparable for each wire type as well as among the four sets of wires.

The $Ni_{49.5}Ti_{50.5}$ data show a minimum in tensile plateau stress at 23 °C compared with tests at −25 °C or at 60 °C. This

Table 2 – ABAQUS UMAT parameters.

Abaqus superelasticity UMAT constants	Symbol	Extracted values
Austenite elasticity (MPa)	E_A	51,437
Austenite poissons ratio	υ_A	0.33
Martensite elasticity (MPa)	E_M	21,588
Martensite poissons ratio	υ_M	0.33
Transformation strain	ε^L	0.037
ds/dT loading (MPa/°C)	$\left(\frac{\delta\sigma}{\delta T}\right)_L$	5.1
Start transformation loading (MPa)	σ_L^S	494
End transformation loading (MPa)	σ_L^E	557
Reference temperature	T_0	22
ds/dT unloading (MPa/°C)	$\left(\frac{\delta\sigma}{\delta T}\right)_U$	5.1
Start transformation unloading (MPa)	σ_U^S	336
End transformation unloading (MPa)	σ_U^E	311
Start transform stress compression (MPa)	σ_{CL}^S	755
Volumetric transformation strain	ε_V^L	0
Number annealing steps	N_A	0
Number of stress–strain pairs	N_P	4
Stress in yield curve (MPa)	σ_1^P	1233
Strain in yield curve	ε_1	0.093
Stress in yield curve (MPa)	σ_2^P	1341
Strain in yield curve	ε_2	0.099
Stress in yield curve (MPa)	σ_3^P	1432
Strain in yield curve	ε_3	0.106
Stress in yield curve (MPa)	σ_4^P	1531
Strain in yield curve	ε_4	0.119

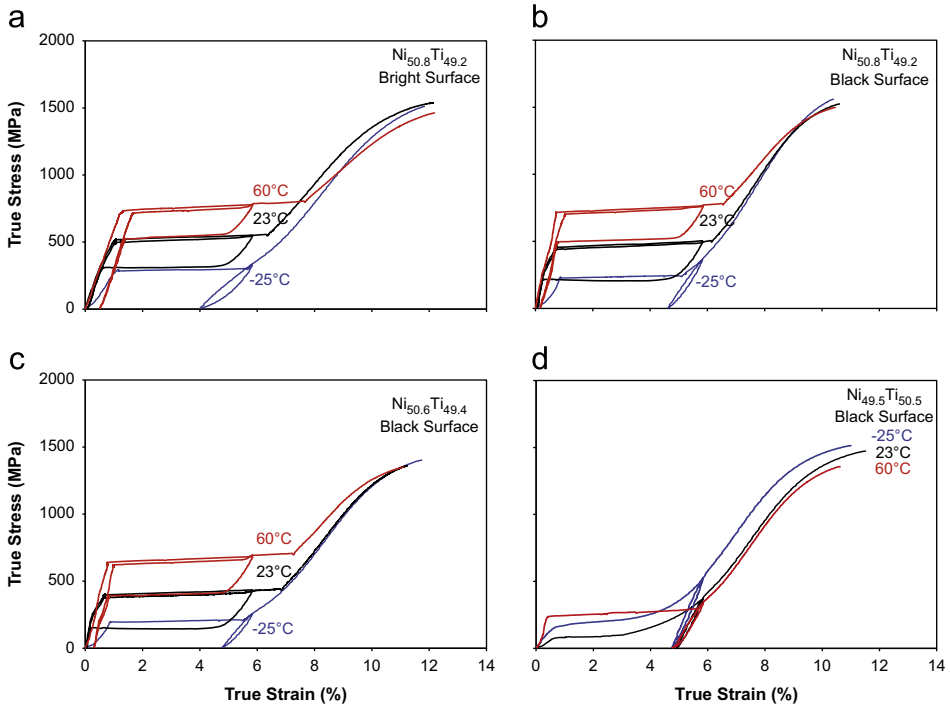

Fig. 2 – Uniaxial tensile behavior of (a) $Ni_{50.8}Ti_{49.2}$ Bright, (b) $Ni_{50.8}Ti_{49.2}$ Black, (c) $Ni_{50.6}Ti_{49.4}$ Black and (d) $Ni_{49.5}Ti_{50.5}$ Black, at −25, 23, 60 °C. Note that the plateau stresses of the three Ni-rich alloys increase with increasing test temperature and have similar characteristics at each temperature. The $Ni_{49.5}Ti_{50.5}$ wire tested at 23 °C has the lowest plateau stress due to the presence of R-phase (see Fig. 3).

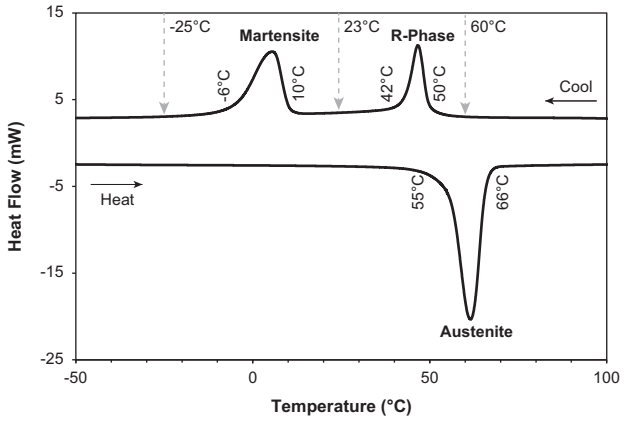

Fig. 3 – Thermogram from DSC test of $Ni_{49.5}Ti_{50.5}$ wires with phase transformation start and finish temperatures as well as peak phase identification noted. Also shown are the three test temperatures for tensile and bending fatigue. The cooling (top) curve dictates the phases for the testing for the −25 and 23 °C tests whereas the heating curve (bottom) shows the phases for the 60 °C tests.

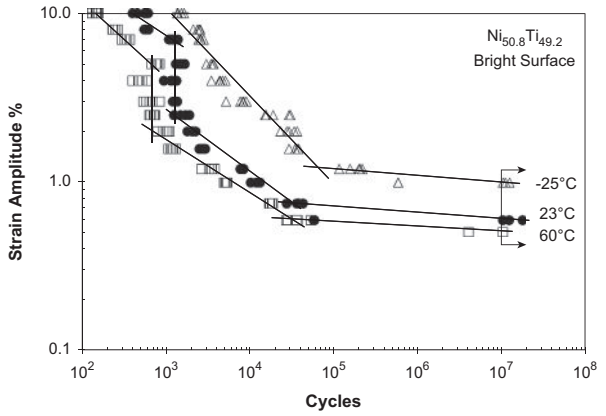

Fig. 4 – Strain amplitude versus number-of-cycles curves for $Ni_{50.8}Ti_{49.2}$ bright wire tested at −25 °C, 23 °C, and 60 °C. Data at ≥10^7 cycles did not fracture and are considered run-out conditions. Trend lines from regression analyses are drawn to delineate strain amplitude regions for these three sets of data.

apparent discrepancy is due to the presence of the R-phase[2] at room temperature. A differential scanning calorimetric (DSC) thermogram of the $Ni_{49.5}Ti_{50.5}$ wire, shown in Fig. 3, illustrates the test temperatures and phases as well as transformation start and finish temperatures. These Ti-rich wires were heated to ~100 °C prior to tensile or rotary bend fatigue tests, so the temperature–phase relationships for the −25 °C and 23 °C tests are dictated by the DSC cooling curve (top). However, the cooling rate was high enough to allow the wires to cool prior to heating for the 60 °C test; therefore, the DSC heating curve (bottom) better reflects the phase content for these tests.

[2]R-phase is considered a martensitic phase (Otsuka and Ren, 2005 with trigonal symmetry ($P\bar{3}$) (Khalil-Allafi et al., 2006.

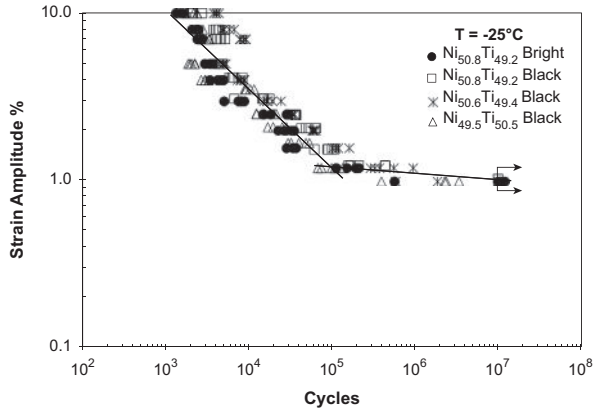

Fig. 5 – Strain amplitude versus number-of-cycles curves at a test temperature of −25 °C for $Ni_{50.8}Ti_{49.2}$ bright, $Ni_{50.8}Ti_{49.2}$ black, $Ni_{50.6}Ti_{49.4}$ black, and $Ni_{49.5}Ti_{50.5}$ black wires. The $Ni_{50.8}Ti_{49.2}$ bright surface data and trend lines from Fig. 4 are re-plotted in this figure for comparison. Data at ≥10^7 cycles are considered run-out conditions.

3.2. *Fatigue of $Ni_{50.8}Ti_{49.2}$ bright wire*

Fig. 4 shows strain amplitude vs. cycles fatigue data for the $Ni_{50.8}Ti_{49.2}$ bright wires tested at −25, 23, and 60 °C plotted on a log–log plot. These data show that fatigue behavior is strongly influenced by test temperature, whereby testing at −25° C (R-Phase) provides the longest lives at the intermediate-to-high strain amplitudes as well as the greatest strain amplitude (1%) at 10^7 cycles. The 60 °C (austenite) fatigue data, on the other hand, has the shortest low-cycle lives and lowest strain amplitude (0.5%) at 10^7 cycles. Trend lines from regression analyses are drawn to delineate strain amplitude regions for these three sets of data. Note that there are four distinct regions for the pseudoelastic conditions (i.e., test temperatures of 23 and 60 °C) whereas there are only two regions at −25 °C. Clearly, the differences between the fatigue conditions reflect the tensile behavior of the wires shown in Fig. 2. The fatigue data from the separate regions are denoted **Region I** ($N \leq 10^3$ cycles for the greatest strain amplitudes), **Region II** ($N \sim 10^3$ cycles), **Region III** ($10^3 \leq N \leq 10^5$ cycles for intermediate strain amplitudes), and **Region IV** ($10^5 \leq N \leq 10^7$ cycles for the lowest strain amplitudes). These characteristics will be discussed below in more detail. In the next sections we will compare the fatigue data from the various wire conditions at the three test temperatures.

3.3. *Fatigue at −25 °C*

Fatigue data for the four material conditions are shown in Fig. 5 at −25 °C test temperature. The $Ni_{50.8}Ti_{49.2}$ bright surface data and trend lines from Fig. 4 are re-plotted in this figure for comparison. Remarkably, the data for all wires show similar behavior at comparable strain amplitudes (see Table 3 for statistical analyses) and the monotonic stress–strain behavior dictates the overall fatigue response since there is no stress-induced martensite transformation that occurs. The strain-life plot appears similar to a typical, non-transforming metallic alloy. All three of the Ni-rich compositions are in the R-phase region, whereas the $Ni_{49.5}Ti_{50.5}$ wire is fully martensitic at −25 °C

Table 3 – Summary of power-law fatigue analysis.

Temperature (°C)	Region I		Region III		Region IV	
	β	R^2	β	R^2	β	R^2
$Ni_{50.8}Ti_{49.2}$ bright wire						
−25			−0.52	0.93	−0.04	0.67
23	−0.32	0.69	−0.32	0.97	−0.03	0.49
60	−0.42	0.99	−0.31	0.97	−0.03	0.99
$Ni_{50.8}Ti_{49.2}$ black wire						
−25			−0.47	0.92	−0.05	0.97
23	−0.56	0.53	−0.33	0.97	−0.03	0.43
60	−0.43	0.98	−0.30	0.92	−0.03	0.42
$Ni_{50.6}Ti_{49.4}$ black wire						
−25			−0.49	0.86	−0.05	0.61
23	−1.16	0.52	−0.35	0.92	−0.05	0.91
60	−0.54	0.89	−0.38	0.94	−0.04	1.00
$Ni_{49.5}Ti_{50.5}$ black wire						
−25			−0.48	0.83	−0.05	0.82
23			−0.62	0.93	−0.09	0.98
60			−0.71	0.89	−0.07	0.86

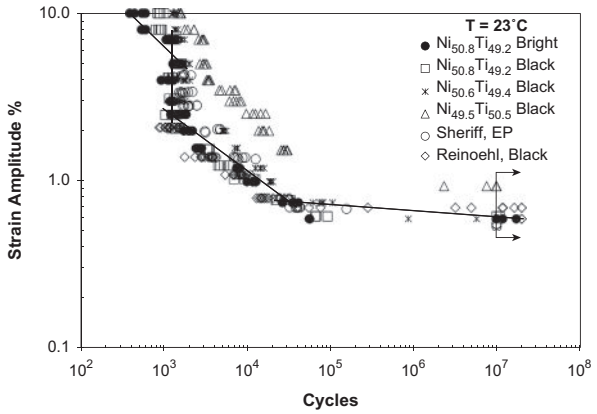

Fig. 6 – Strain amplitude versus number-of-cycles curves at a test temperature of 23 °C for $Ni_{50.8}Ti_{49.2}$ bright, $Ni_{50.8}Ti_{49.2}$ black, $Ni_{50.6}Ti_{49.4}$ black and $Ni_{49.5}Ti_{50.5}$ black wires. Also included in this figure are data from Sheriff et al. from for $Ni_{50.8}Ti_{49.2}$ electropolished wires (Sheriff and Pelton, 2005) and from $Ni_{50.8}Ti_{49.2}$ black wires with two ingot sources (Reinoehl et al., 2001). The $Ni_{50.8}Ti_{49.2}$ bright surface data and trend lines from Fig. 4 are re-plotted in this figure for comparison. Data at $\geq 10^7$ cycles are considered run-out conditions.

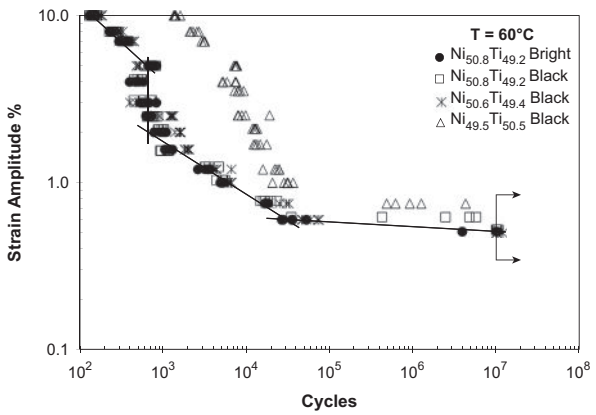

Fig. 7 – Strain amplitude versus number-of-cycles curves at a test temperature of 60 °C for $Ni_{50.8}Ti_{49.2}$ bright, $Ni_{50.8}Ti_{49.2}$ black, $Ni_{50.6}Ti_{49.4}$ black, and $Ni_{49.5}Ti_{50.5}$ black wires. The $Ni_{50.8}Ti_{49.2}$ bright surface data and trend lines from Fig. 4 are re-plotted in this figure for comparison. Data at $\geq 10^7$ cycles are considered run-out conditions.

(as indicated in Fig. 3). The 10^7-cycle fatigue strain limit is 1% under these test conditions.

3.4. *Fatigue at 23 °C*

The fatigue data for the four material conditions are shown in Fig. 6 at the 23 °C test temperature. The $Ni_{50.8}Ti_{49.2}$ bright data and trend lines from Fig. 4 are re-plotted in this figure for comparison. The $Ni_{50.8}Ti_{49.2}$ black and $Ni_{50.6}Ti_{49.4}$ black wires also follow similar trends to $Ni_{50.8}Ti_{49.2}$ bright wire data. For comparison, $Ni_{50.8}Ti_{49.2}$ wire fatigue data from Reinoehl et al., (2001) (black) and Sheriff and Pelton (2005) (electropolished) are also shown in this figure. The $Ni_{49.5}Ti_{50.5}$ wires (R-Phase) showed longer lives in the low-cycle fatigue region and a greater fatigue strain limit in the high-cycle fatigue region.

3.5. *Fatigue at 60 °C*

The fatigue data for the four material conditions are shown in Fig. 7 at 60 °C. The $Ni_{50.8}Ti_{49.2}$ bright surface data and trend lines from Fig. 4 are re-plotted in this figure for comparison. Note that the data for the $Ni_{50.8}Ti_{49.2}$ bright and black surface conditions as well as the $Ni_{50.6}Ti_{49.4}$ black fall on top of each other, indicating that there is no significant difference between these surface conditions. In contrast, the $Ni_{49.5}Ti_{50.5}$ wires showed longer lives in the low-cycle fatigue region and a greater fatigue strain limit in the high-cycle fatigue region. As shown on the DSC curve in Fig. 3 the Ti-rich wires contain a two-phase mixture of austenite and martensite at 60 °C.

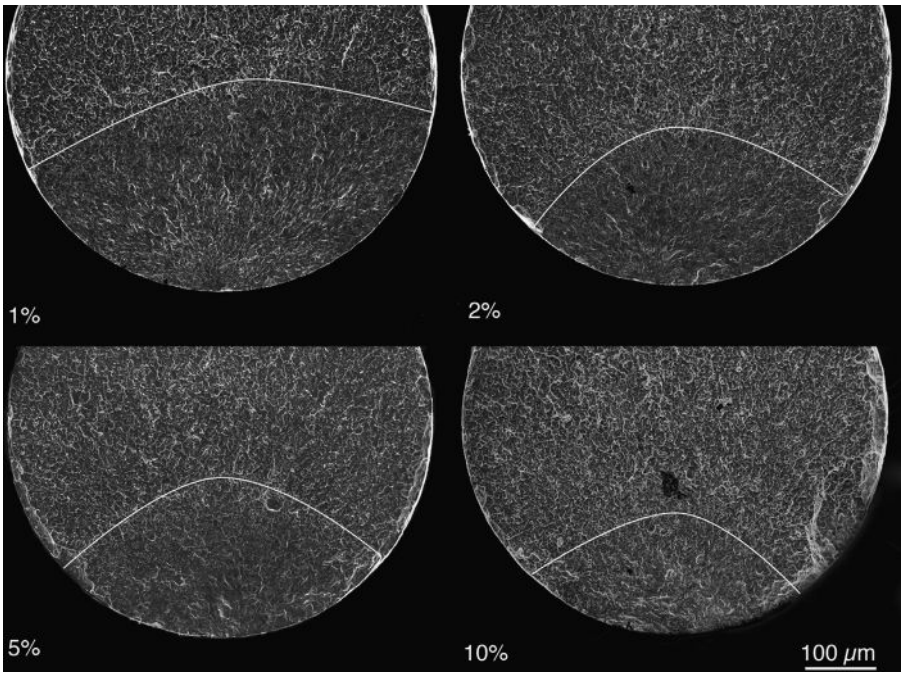

Fig. 8 – SEM images of the fracture surfaces for $Ni_{50.8}Ti_{49.2}$ bright wire tested at room temperature at strain amplitudes of 1% (11,931 cycles, Region IV**), 2% (2039 cycles,** Region III**), 5% (1487 cycles,** Region II**) and 10% (520 cycles,** Region I**). Note that the size of the fatigue fracture area increases as the strain amplitude decreases.**

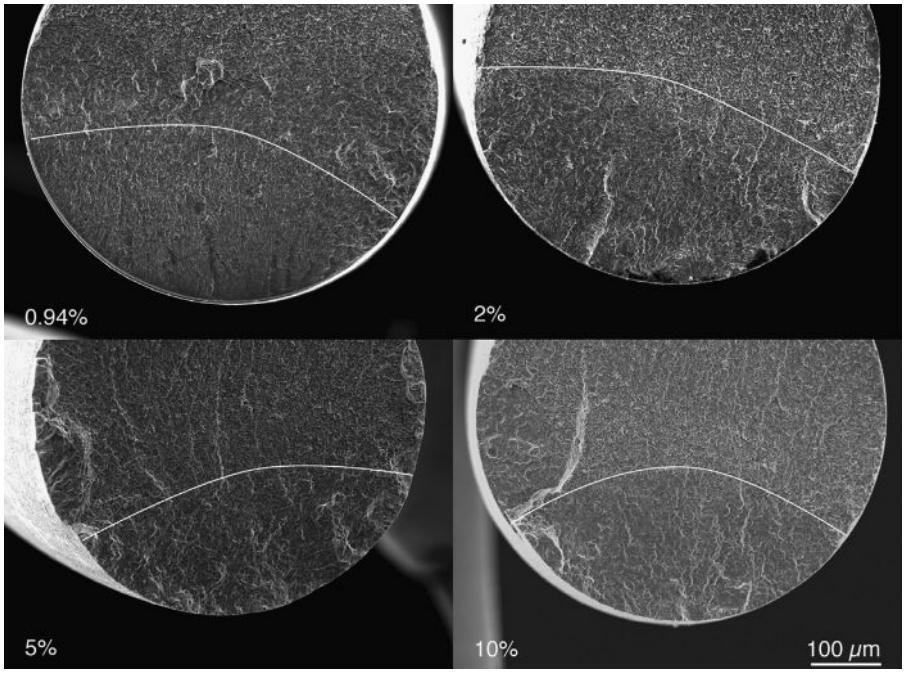

Fig. 9 – SEM images of the fracture surfaces for $Ni_{49.5}Ti_{50.5}$ black wire tested at room temperature at strain amplitudes of 0.94% (7,946,029 cycles), 2% (16,031 cycles), 5% (3084 cycles) and 10% (1546 cycles).

3.6. *Fracture surfaces*

SEM images of the fracture surfaces are shown in Figs. 8 and 9 for the $Ni_{50.8}Ti_{49.2}$ bright wire and $Ni_{49.5}Ti_{50.5}$, respectively, at four strain amplitudes that correspond to the four superelastic fatigue regions: **Region IV** – 1%, **Region III** – 2%, **Region II** – 5%, and **Region I** – 10%.

4. Discussion

4.1. *Monotonic and bending mechanical properties*

The uniaxial tensile properties of the Nitinol wires shown in Fig. 2 can be used as an approximate guide for the cyclic bending behavior. However, there are a number of differences that should be considered that limits the ability to quantify the

data. First, the use of mandrels to guide the wires into the defined curvature has the effect of creating a larger region of wire that is subjected to the same strain amplitude. As shown by Berg (1995) and Wick and Vöhringer (1995), pure (unconstrained) bending of pseudoelastic Nitinol creates non-circular arcs on the stress-induced martensite plateau. These macroscopic facets are due to regions that are either deformed austenite or stress-induced martensite. Consequently, it is difficult to ascribe an absolute strain to this transforming region under free rotating bending conditions. Second, Nitinol displays an anisotropy in tension vs. compression behavior. The phenomenological theory of martensitic transformations has been used effectively to model tension-compression asymmetry and the orientation dependence of the deformation behavior of Nitinol (Buchheit and Wert, 1994, 1996; Gall and Sehitoglu, 1999a; Gall and Sehitoglu, 1999b). These analyses show that the martensite variants created in tension are different from those created in compression, which give rise to differences in plateau stresses, shape memory recovery strains, and critical resolved shear stresses. Third, there are few direct experimental comparisons between the tensile and bending properties of Nitinol so calculation of bending curves from uniaxial data is not straightforward. Plasticity theory has been applied to a pseudoelastic beam to estimate bending properties from tension data (Atanacković and Achenbach, 1989; Wick and Vöhringer, 1995). The upper plateau stress in tension, σ_{UP}, and the elastic strain limit, $\varepsilon_{el}=\sigma_{UP}/E$, where E is the elastic modulus, were the only parameters used to calculate the bending stress, σ_b. Wick and Vöhringer demonstrated that the modulus of pseudoelastic Nitinol in tension and bending are equivalent based on extensive investigations under pure- and four-point-bending conditions with strain-gage instrumentation (Wick and Vöhringer, 1995). They further showed that the above relationship worked well to relate the upper plateau stresses from tensile tests to bending stresses and were comparable to the theoretical ratio of 1.7. However, there were significant discrepancies in the calculated unloading plateau stresses compared to the experimental data. Wagner and Eggeler (2006a, 2006b) used numerical calculations to show that the stress and strain states differ significantly between pure bending and bending rotation of pseudoelastic Nitinol wires. However, their models neglected to take into account the tension-compression asymmetry that therefore underestimates the compression stresses. Furthermore, a recent publication by Reedlunn and Churchill (2012) investigated the surface strain evolution of Nitinol tubing (DSC A_f of 19 °C) under tension, compression and bending conditions at room temperature with stereo digital image correlation. Their results clearly showed the asymmetry in uniaxial tension and compression (where their compression plateau stress is ~1.5 × the tension plateau stress). Furthermore, the stress plateau in tension was relatively flat and 5.45% in length whereas in compression the plateau has an upward slope with 3.49% length. Their four-point bending testing provided moment-curvature curves similar to those shown by Wick and Vöhringer (1995) with the bending-tension plateau ratio of ~1.69, also comparable to the theoretical ratio. Furthermore, their model showed reasonable agreement with the bending loading curves predicted from tension-compression data (although they did not predict unloading curves).

4.2. *Finite element analysis*

The commercial non-linear FEA code used in this investigation offers insight into the relative behavior of the wires under rotary bending test conditions. Fig. 10 shows FEA strain contours calculated for the $Ni_{50.8}Ti_{49.2}$ bright wires in cross section for strain amplitudes of 1, 2, 5, and 10% that represent the four distinct strain regions from Fig. 4 at 23 °C. The strain color levels were normalized to the 10% strain amplitude condition, although in each case the compressive strains were greater than the tensile strains. Stress–strain curves for these wires are presented in Fig. 11 from the FEA simulations. These results depict the tension-compression characteristics for the conditions of the cyclic deformation. In agreement with prior tensile-compressive testing of pseudoelastic Nitinol, the compressive stress plateau is 1.5 greater than that of the tensile plateau stress, per defined material parameters. As such, the compressive elastic region is greater than the tensile elasticity. For example, at 1% strain, the tensile conditions lead to a small stress hysteresis whereas on the compressive side of the cycles, the wires are still in the linear elastic region. At 2 and 5% strain amplitudes, the tensile stress hysteresis is again greater than that on the compressive side. At 10% strain amplitude there is approximately 0.7% remnant strain (permanent set) on the tensile cycle unloading, whereas the wire does not reach compressive yield at this strain amplitude. Therefore, based on these FEA curves, it is likely that the compressive cycling leads to greater damage accumulation than tensile cycling due to greater stress amplitude per cycle. Although still under development (Stebner and Bhattacharya, 2013; Stebner and Brinson, 2013), non-linear FEA that takes into account micromechanical modeling of the uniaxial tension and compression behavior may provide a more accurate model of rotating bend fatigue and other multi-axial deformation of Nitinol.

4.3. *Fatigue of $Ni_{50.8}Ti_{49.2}$ bright wire*

We will use the fatigue data from Fig. 4 (as well as the FEA results in Fig. 11) to examine the general trends in fatigue behavior and then compare the effects of test temperature, composition, and surface condition. It is clear that greater temperature differences, ΔT (where ΔT is defined as the difference between deformation temperature and A_f (Pelton and Duerig, 2004)) result in shorter low-cycle fatigue life as well as lower strain amplitudes limits at 10^7 cycles. Trend lines from regression analyses are drawn to delineate strain amplitude regions for these three sets of data; we will first consider the two pseudoelastic conditions for test temperatures of 60 and 23 °C that show four distinct fatigue regions. At the greatest strain amplitudes in **Region I** ($5\% \leq \varepsilon_a \leq 10\%$), the fatigue life decreases with increasing strain amplitude. This strain amplitude regime approximately corresponds to the end of the stress-induced martensite plateau to beyond the martensitic yield point in the monotonic tension-compression curve (refer to Fig. 11d). As such, strain amplitudes in the 5–10% regime represent elastic-plastic deformation of the stress-induced martensite, where the yield strain in tension corresponds to ~10%.

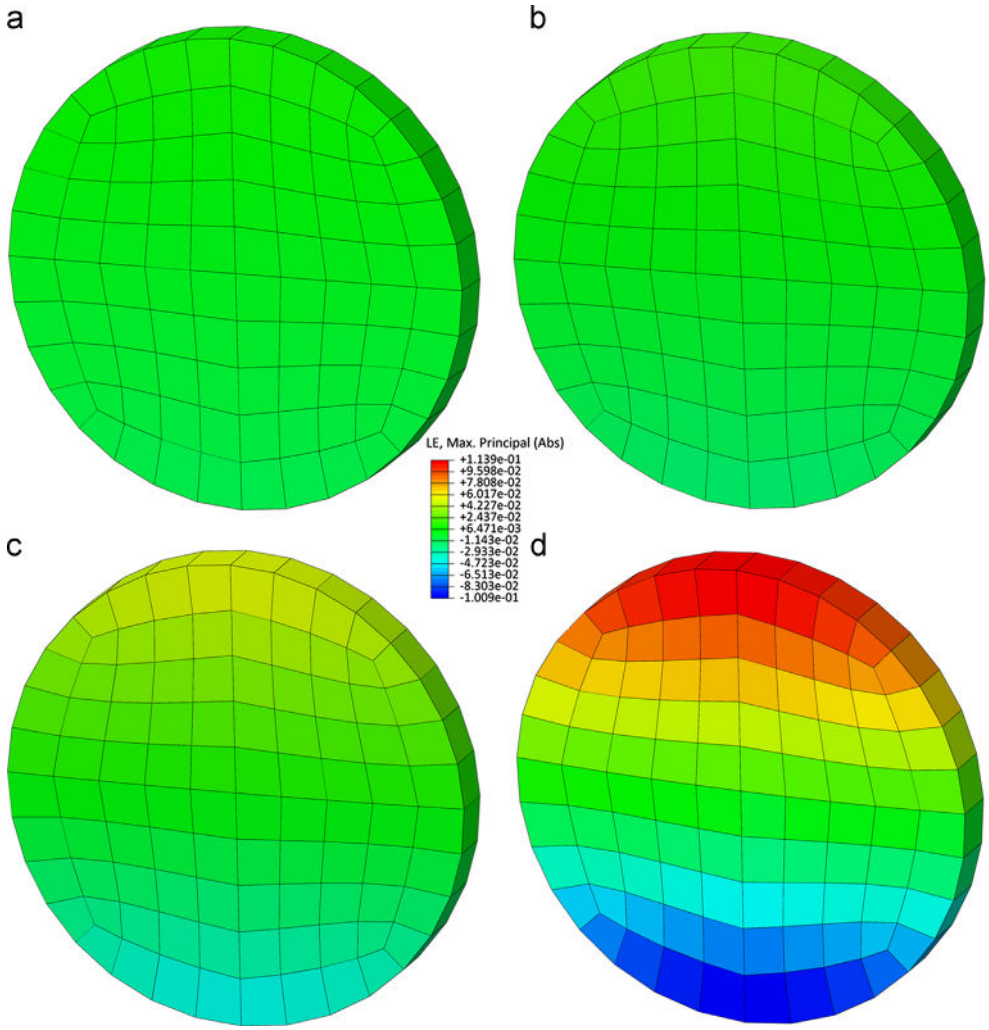

Fig. 10 – Finite element analysis of $Ni_{50.8}Ti_{49.2}$ bright wire at (nominal) strain amplitudes of (a) 1% (Region IV), (b) 2% (Region III), (c) 5% (Region II) and (d) 10% (Region I) at 23 °C. The strains are normalized to those of (d).

These low-cycle fatigue data can be analyzed in accordance with empirical power-law relationships:

$$\varepsilon_\alpha = A(N)^\beta \tag{2}$$

here ε_α is the strain amplitude, A is the intercept for $N=1$ (where: N is the number of cycles), and β is the exponent. Power-law analysis has been used for over a century for analyzing fatigue data in the high-cycle, primarily elastic region (Basquin) (Basquin, 1910) and for over 50 years in the low-cycle plastic region (Coffin–Manson) (Coffin and Tavernelli, 1959; Manson, 1966) for conventional engineering materials. Direct application of the Basquin and Coffin–Manson relationships to Nitinol fatigue leads to uncertainly since the pseudoelastic curves have contributions from elastic, transformational, and plastic strains (Mehta and Gong, 2007; Barney and Xu, 2011). As discussed above, the rotary-bend fatigue tests were not instrumented so that discrete values of stress for the imposed strains and the ability to partition strains are not available. Therefore, for the purpose of comparison among the combinations of composition and surface conditions we will calculate the power-law parameters based on *total* strain amplitudes. The fatigue parameters for each test condition from **Region I**, **Region III**, and **Region IV** are summarized in Table 3.

Strain amplitudes between $2\% \leq \varepsilon_a \leq 5\%$ (60 °C) and $2.5\% \leq \varepsilon_a \leq 7\%$ (23 °C) define **Region II** where there is approximate constant fatigue life at 60 °C the average lifetime is 696 cycles ($s=173$, where s is the standard deviation) and at 23 °C the average lifetime is 1323 cycles ($s=264$). This constant-life trend was noted by Kim and Miyazaki (1997), Miyazaki and Mizukoshi (1999) and Sheriff and Pelton (2005), albeit at lower strain amplitudes, and was attributed to the effects of stress-induced martensitic transformations. Monotonic bending experiments for Nitinol wire under pure and four-point bend modes at room temperature indicate that the onset of the stress-induced martensite begins at ~2% strain compared with a tensile onset of ~1% (Wick and Vöhringer, 1995), comparable to the 23 °C data for these wires. Consequently, wires that are deformed under these conditions are subjected to approximate constant tensile and compressive stresses (see Fig. 11c). At −25 °C ($\Delta T=-89$ °C), the $Ni_{50.8}Ti_{49.2}$ wires have an R-Phase structure and therefore do not show this region of constant life.

Region III of the pseudoelastic curves shows an increasing fatigue life with decreasing strain amplitude, corresponding to

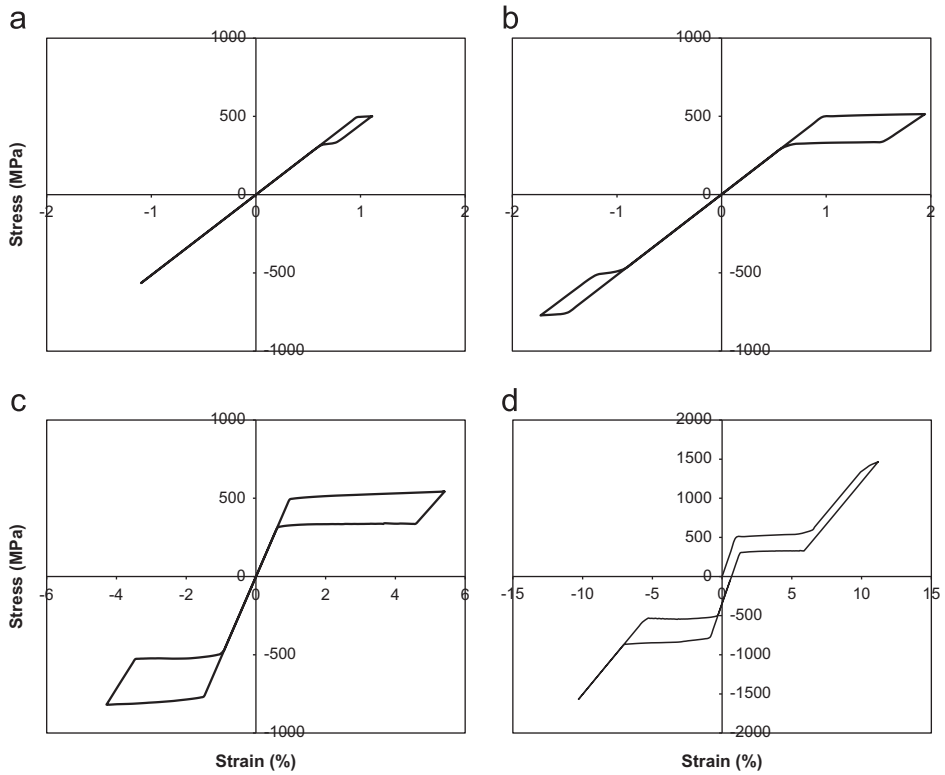

Fig. 11 – Finite element analysis of $Ni_{50.8}Ti_{49.2}$ bright wire at (nominal) strain amplitudes of (a) 1% (Region IV), (b) 2% (Region III), (c) 5% (Region II) and (d) 10% (Region I) at 23 °C. The stress and strain scales are selected to accentuate the differences in tension and compression at each strain amplitude.

strain amplitudes between 2% and 0.6% (60 °C) and 2.5% and 0.75% (23 °C). It is interesting that the power-law exponent from the (non-transforming) −25 °C data is approximately −0.5, comparable in magnitude to the Coffin–Manson exponents for many engineering materials (Suresh, 1998). In contrast, the exponents for the pseudoelastic conditions are lower and range from −0.38 to −0.30. Clearly, these differences in exponents indicate differences in cyclic deformation mechanisms, whereby at −25 °C there is no stress-induced martensitic transformation and therefore represents an elastic-plastic fatigue mechanism. For the $Ni_{50.8}Ti_{49.2}$ and $Ni_{50.6}Ti_{49.4}$ wires tested at 23° C and 60 °C, there is a distinct stress-induced phase transformation in the tensile curves in Figs. 2 and 11b. This region therefore represents both elastic and transformational strains.

Region IV represents the high-cycle data ($N \geq 10^5$ cycles) with strain amplitudes of 0.6–0.5% (60 °C), 0.75–0.6% (23 °C), and 1.2–1.0% (−25 °C). All data at $\geq 10^7$ cycles did not fracture and are considered run-out conditions. This strain amplitude region is consistent with elastic cyclic deformation at each test temperature, as shown in Figs. 2 and 11a. It is assumed that the fatigue mechanism under these conditions is due to typical non-transformational damage accumulation in this (nominally) linear–elastic region (Suresh, 1998). The exponent ranges from −0.03 to −0.07, which are equivalent in magnitude to Basquin exponents obtained in conventional engineering materials (Suresh, 1998); clearly these low strain amplitudes correspond to elastic deformation of single-phase material with no stress-induced phase transformation.

The 60 °C high-cycle data show the lowest strain amplitude of 0.5% at 10^7 cycles, whereas at 23 °C, the corresponding value is 0.6%, and at −25 °C, the value is 1.0%; the 10^7-cycle strain amplitudes for the four wires and three test temperatures are shown in Figs. 12 and 13 as a function of the ΔT and elastic modulus, respectively. These figures show the general trend that the 10^7-cycle fatigue strain limit for pseudoelastic Nitinol increases with decreases in both ΔT and modulus of elasticity. Note that these figures reflect that there is a 10^7-cycle fatigue strain limit of 1% for conditions of $\Delta T \leq -40$ °C and $E \leq 20$ GPa, consistent with the results in Fig. 5. As such, it appears that R-Phase and thermal martensite have similar fatigue behavior under these testing conditions. Fig. 12 also shows recent data from Gupta and Weaver (2013) of thermomechanically treated electropolished Nitinol wires (A_f 16 °C) that were tested at 37 °C (circle symbol) with run out strain amplitude of 0.6%. The ΔT value of their tests is 21 °C, which is identical to that of the $Ni_{50.8}Ti_{49.2}$ bright wires tested at RT. This comparison supports the predictive relationship of ΔT on the fatigue strain limits, whereby the difference in A_f and test temperature is a controlling factor on fatigue behavior. Furthermore, the data in Figs. 12–13 suggest that for a given strain amplitude the stress amplitude decreases with decreasing ΔT and decreasing E with a concomitant increase in fatigue strain limit. Consequently, it is not surprising that the high-cycle fatigue data at 23 °C test temperature is greater than those at 60 °C. Therefore, the optimal fatigue behavior for pseudoelastic conditions may be obtained when the A_f temperature is comparable to the test temperature.

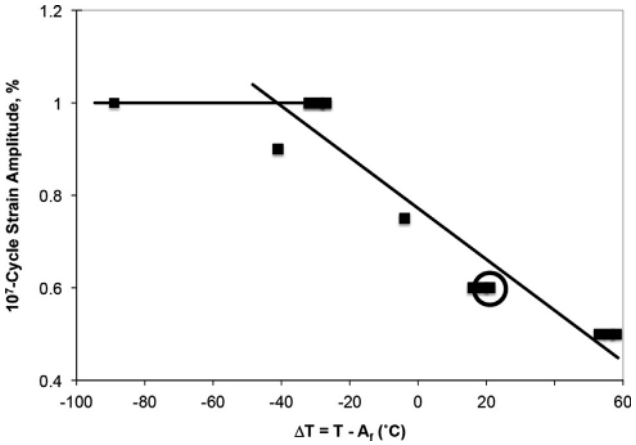

Fig. 12 – Effect of ΔT on the fatigue strain limit at 10^7 cycles for the four wires and three test temperatures. Note that there is a dramatic increase in fatigue strain limit with decreasing ΔT. According to the data in this investigation, the limit in the fatigue strain amplitude occurs under conditions of martensite (R-Phase or B19'). For superelastic applications, these data substantiate that improved fatigue behavior is obtained when the A_f is set as close as possible to the test temperature. Also shown on this figure are the rotary bending results (circle symbol) from Gupta and Weaver (2013) who tested electropolished Nitinol wire with A_f 16 °C at 37 °C (ΔT=21 °C). Note that their results are identical to the $Ni_{50.8}Ti_{49.2}$ bright wire also with ΔT=21 °C.

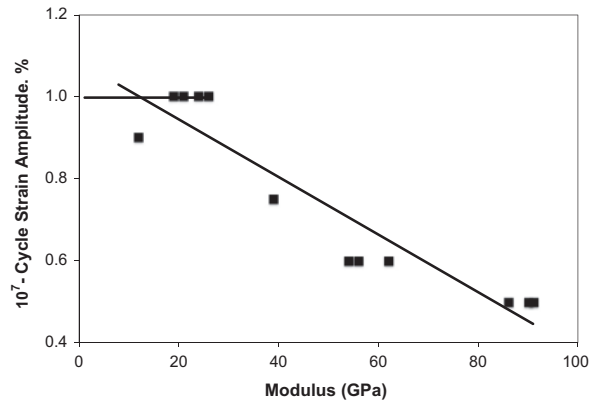

Fig. 13 – Effect of (initial) modulus on the fatigue strain limit at 10^7 cycles for the four wires and three test temperatures. Note that there is a dramatic increase in fatigue strain with decreasing modulus.

As discussed in previous publications, mechanistically, it is not known if the fatigue behavior observed in pseudoelastic Nitinol is due to microstructural effects of martensite (i.e., formation of stabilized martensite during cycling with the incorporation of plasticity) or rather to the lower moduli associated with the stress-induced transformation regime (i.e., decreased hysteresis energy) (Pelton and Schroeder, 2008; Robertson and Pelton, 2012).

The four sets of pseudoelastic data are consistent with each other and have shorter fatigue lives at equivalent strain amplitudes compared with the thermal martensite results up to 4.3% strain amplitude. From Fig. 4 it is shown that for a given strain amplitude, the stress required to deform R-Phase is less than those required to stress-induce martensite under pseudoelastic conditions. Furthermore, it has been shown that the crack-growth rates for thermal martensite and pseudoelastic material are virtually identical (Robertson and Pelton, 2012); therefore, under strain-controlled conditions it appears that the crack initiation rates are faster in the pseudoelastic condition than in thermal martensite. The area within the hysteresis loops is a measure of work and therefore can be modeled in an analogous manner to account for damage accumulation due to the effects strain amplitude. For pseudoelastic cycling, these models are consistent with decreasing elastic energy with increasing cycles due to the increase of internal elastic stress field in the direction of the applied stress resulting from creation and rearrangement of dislocations and deformed martensite (Pelton, 2011). Smith–Watson–Topper (SWT) (Smith and Watson, 1970) developed a phenomenological fatigue model in which they hypothesized a generalized stress–strain function to predict fatigue life and assumed that the function should be applicable to crack initiation and at least the early part of crack propagation. Their function is based on determining the stress range ($\Delta\sigma$), strain range ($\Delta\epsilon$) and modulus of elasticity (E). One version of this relationship for strain-controlled tests can be stated as $P^{SWT} = \sqrt{\sigma_{max}\Delta\varepsilon E}$. From this simple relationship, it can be seen that the fatigue parameter (P^{SWT}) is minimized with minimal values of stress, strain, and modulus. Such a presentation also eliminated the necessity of accounting for a mean stress that may develop during cycling particularly at large tensile or compressive mean strain-type deformations common to deployed Nitinol medical implants. However, complications arise when Nitinol fatigue data are analyzed with SWT since the strain amplitudes are well beyond the initial linear–elastic range where the conventional E is valid; for each strain condition there is another effective modulus due to the coexistence of austenite and martensite. Therefore the SWT parameter can be modified to include only the product of stress and strain, as was done to analyze Nitinol thermal fatigue data under conditions of a constant applied force (Proft and Melton, 1989). This approach is particularly convenient because this measure of the work-per-cycle is comparable to thermodynamic analyses of Nitinol fatigue (Patoor and Barbe, 1991; Liu and McCormick, 1994; McCormick and Liu, 1994). Furthermore, as demonstrated by the early work of Melton and Mercier (1979) mechanical cycling of Nitinol under R=−1 conditions leads to decreasing hysteresis and ultimately an approximate linear deformation from which an effective modulus can be determined. While it is beyond the scope of this present work, a finite element model that extracts the full stress/strain history during the duty cycle, including the change in hysteresis would be useful to predict Nitinol behavior under a variety of fatigue conditions.

4.4. *Effects of surface finish and microstructure*

The effects of surface finish on the fatigue of Nitinol can be evaluated by comparing the data in Fig. 6 where black oxide, bright mechanical polish, and electropolished wires (Sheriff and

Pelton, 2005) with similar processing conditions and resultant A_f temperatures are shown. Electropolishing is an electrochemical process that removes surface oxides (and other surface contaminants, such as lubrication, as well as surface scratches from wire drawing) and creates a smooth and bright surface. In the low-cycle fatigue regime (**Regions II–III**), electropolished wire resulted in a slight increase in fatigue life; however, there is no significant difference in the high-cycle fatigue regime for the three wire surface finishes. Gupta and Weaver (2013) investigated the influence of bending pre-strain on the rotary bending fatigue behavior of electropolished 0.5 mm diameter Nitinol wire (A_f 16 °C) tested at 37 °C between 0.3% and 1.5% strain amplitude to 10^8 cycles. Their baseline wires (no pre-strain) showed similar trends as the (Sheriff and Pelton, 2005) electropolished data with run out strain limit of 0.6%. Furthermore, Cheung and Shen (2007) observed no discernible difference in fatigue behavior between electropolished and machined Nitinol dental files ($p>0.05$) that were tested under rotary bending conditions. They observed that although surface smoothness was enhanced by electropolishing, this did not protect the instrument from fatigue fracture.

The influence of surface finish (and especially the benefits of electropolishing) has been discussed for laser-machined Nitinol stents (see, for example, Smouse and Nikanorov (2005) and references therein). In contrast to wire-based Nitinol devices, the major influence of surface processing on in vivo fatigue behavior of laser-machined tubing-based components is to remove heat-affected zones and possible surface defects that could initiate a fatigue crack. Consequently, comparable fatigue studies of laser-machined Nitinol components would likely demonstrate more pronounced differences than observed in this investigation.

Since fatigue of both thermal martensite and pseudoelastic austenite material requires crack propagation through a martensitic phase, one would expect similarities between the fracture surfaces. Figs. 8–9 show fracture surfaces in these two-phase conditions tested under four strain–amplitude conditions. As expected, both phases produced rough fracture topography in the low-cycle (5% and 10% strain amplitudes) condition. Indeed, 10% strain conditions lead to unstable crack growth with fatigue-crack propagation through only a small percentage of the cross-section prior to complete ductile overload failure (see line delimiting the regions). Conversely, under the high cycle 1% strain–amplitude condition, the thermal martensite sample (Fig. 9a) is able to sustain approximately 50% stable crack growth over ~10^7 cycles resulting in a relatively flat fracture through the sample before ductile overload fracture ensued. The same 1% alternating strain input to the pseudoelastic material (Fig. 8a) resulted in medium-cycle (~10^5) fatigue fracture. Interestingly, the pseudoelastic austenite samples tested at both 1% and 10% strain amplitudes show similar surface roughness typical of the fast fatigue fracture and/or final ductile overload event. Because the two samples have significantly different fatigue lifetimes but similar fracture surfaces, it suggests that the majority of the fatigue lifetime in these pseudoelastic austenitic Nitinol samples is spent in crack nucleation rather than stable crack growth. Furthermore, it is well known that fatigue cracks initiate at inclusions (oxides and carbides) that are inherent in Nitinol. A more complete analysis of the effects of Nitinol purity and inclusions on crack initiation will be discussed in a forthcoming paper (Launey and Robertson, 2012).

5. Conclusions

This research investigated the rotary bending fatigue characteristics of Nitinol wires with three compositions and two surface finishes under zero-mean strain conditions. The following trends were observed in this study:

1. Under rotating strain-controlled conditions, test temperature and A_f temperature strongly affect the fatigue lives of Nitinol wires under rotary bending cyclic conditions. Lower test temperatures and higher A_f temperatures (lower ΔT) lead to longer lives and greater fatigue strain limits to 10^7 cycles. The wire surface finish (black and bright) had a limited effect on fatigue life under these test conditions.
2. Four distinct regions were observed in the pseudoelastic fatigue data, consistent with proposed mechanisms of cyclic strain accommodation. In the low-cycle region (Region I), fatigue life decreases with increasing strain amplitude between approximately 5–10%; this range corresponds to the strains greater than the end of the stress plateau. In **Region II** (~2–7% strain amplitude) the fatigue life of the wires was independent of strain, consistent with a mechanism of transforming austenite to stressed-induced martensite with approximately constant tension and compression stresses. In the **Region III** strain range, fatigue life increases with decreasing strain amplitude. Data in this region can be analyzed with a modified Coffin–Manson coefficient that tended to decrease as ΔT increases. This strain range is a transition region between linear elastic and transforming austenite and mechanistically is likely to be the most complicated. The high-cycle strain range in **Region IV** corresponds most closely to a traditional linear–elastic fatigue and can be analyzed with a Basquin model.
3. In contrast to the stress-transforming conditions, thermal martensite (R-phase and B19') exhibited only two regions: **Region IV** with strain amplitudes ≤1.2% ($N \geq 10^5$–10^7 cycles) and **Region III** with strain amplitudes ≥1.2% ($N \leq 10^5$ cycles).
4. FEA demonstrates the differences in tension and compression components of the fatigue conditions for rotating bending. These results indicate that for a given strain amplitude, the compression component undergoes greater stress amplitudes with greater damage accumulation.

REFERENCES

ASTM, 2005. Standard Specification for Wrought Nickel–Titanium Shape Memory Alloys for Medical Devices and Surgical Implants. ASTM International F 2063-05.

ASTM, 2006. Standard Test Method for Determination of Transformation Temperature of Nickel-Titanium Shape Memory Alloys by Bend and Free Recovery. ASTM International F 2082-06.

ASTM, 2006. Standard Test Method for Tension Testing of Nickel-Titanium Superelastic Materials. ASTM International F 2516-06.
Atanacković, T., Achenbach, M., 1989. Moment-curvature relations for a pseudoelastic beam. Continuum Mechanics and Thermodynamics 1 (1), 73–80.
Bahia, M.G.A., Martins, R.C., et al., 2005. Physical and mechanical characterization and the influence of cyclic loading on the behaviour of nickel-titanium wires employed in the manufacture of rotary endodontic instruments. International Endodontic Journal 38 (11), 795–801.
Barney, M.M., Xu, D., et al., 2011. Impact of thermomechanical texture on the superelastic response of Nitinol implants. Journal of the Mechanical Behavior of Biomedical Materials 4 (7), 1431–1439.
Basquin, O., 1910. The exponential law of endurance tests. ASTM Proceedings 10, 625–630.
Berg, B.T., 1995. Bending of superelastic wires, Part I: experimental aspects. Journal of Applied Mechanics 62 (2), 459–465.
Bhattacharya, K., 2003. Microstructure of Martensite. Oxford University Press, Oxford.
Buchheit, T., Wert, J., 1994. Modeling the effects of stress state and crystal orientation on the stress-induced transformation of NiTi single crystals. Metallurgical and Materials Transactions A 25 (11), 2383–2389.
Buchheit, T., Wert, J., 1996. Predicting the orientation-dependent stress-induced transformation and detwinning response of shape memory alloy single crystals. Metallurgical and Materials Transactions A 27 (2), 269–279.
Cheung, G.S.P., Shen, Y., et al., 2007. Does electropolishing improve the low-cycle fatigue behavior of a nickel–titanium rotary instrument in hypochlorite?. Journal of Endodontics 33 (10), 1217–1221.
Coffin, J.L.E., Tavernelli, J.F., 1959. The cyclic straining and fatigue of metals. Transactions of the American Institute of Mining Engineers 215, 794–807.
Dessault Systèmes. UMAT and VUMAT Routines for the Simulation of Nitinol, Simulia SOSS Answer ID 1658, Dassault Systèmes Simulia Corp., Providence, RI.
Drexel, M., Selvadury, G., et al., 2008. The effects of cold work and heat treatment on the properties of Nitinol wire. In: Berg, B., Mitchell, M.R., Proft, J. (Eds.), Proceedings of International Conference on Shape Memory and Superelastic Technologies, pp. 447–454.
Duerig, T., Pelton, A., et al., 1999. An overview of Nitinol medical applications. Materials Science and Engineering A 273–275, 149–160.
Gall, K., Sehitoglu, H., 1999a. The role of texture in tension-compression asymmetry in polycrystalline NiTi. International Journal of Plasticity 15 (1), 69–92.
Gall, K., Sehitoglu, H., et al., 1999b. Tension-compression asymmetry of the stress-strain response in aged single crystal and polycrystalline NiTi. Acta Materialia 47 (4), 1203–1217.
Graham, R., VanDoren B., et al., 2004. Characteristics of high purity Nitinol. In: Pelton, A.R., Duerig, T., (Eds.), Proceedings of the Fourth International Conference on Shape Memory and Superelastic Technologies (SMST) 2003, Pacific Grove, CA, International Organization on SMST, pp. 7–14.
Gupta, S., Weaver, J., et al., 2013. High Compressive Prestrain Reduces Fatigue Life of Electropolished Nitinol Wire. SMST 2013. ASM International, Prague, CZ.
Khalil-Allafi, J., Schmahl, W.W., et al., 2006. Space group and crystal structure of the R-phase in binary NiTi shape memory alloys. Acta Materialia 54 (12), 3171–3175.
Kim, Y., S. Miyazaki, 1997. Fatigue life of Ti–50 at% Ni and Ti–40Ni–10Cu (at%) shape memory alloy wires. Shape Memory and Superelastic Technologies-97, SMST, Asilomar, CA.
Launey, M., S.W. Robertson, et al., 2012. Role of Inclusions on the Fatigue Resistance of Nitinol.
Liu, Y., McCormick, P.G., 1994. Thermodynamic analysis of the martensitic transformation in NiTi—I. Effect of heat treatment on transformation behaviour. Acta Metallurgica et Materialia 42 (7), 2401–2406.
Manson, S., 1966. Thermal Stress and Low Cycle Fatigue. McGraw-Hill, New York125–192.
McCormick, P.G., Liu, Y., 1994. Thermodynamic analysis of the martensitic transformation in NiTi—II. Effect of transformation cycling. Acta Metallurgica et Materialia 42 (7), 2407–2413.
Mehta, A., Gong, X.-Y., et al., 2007. Understanding the deformation and fracture of Nitinol endovascular stents using in situ synchrotron X-ray micro-diffraction. Advanced Materials 19 (May), 1183–1186.
Melton, K.N., Mercier, O., 1979. Fatigue of NITI thermoelastic martensites. Acta Metallurgica 27 (1), 137–144.
Miyazaki, S., Mizukoshi, K., et al., 1999. Fatigue life of Ti-50 at% Ni and Ti–40Ni–10 Cu (at%) shape memory alloy wires. Materials Science and Engineering A 273–275, 658–663.
Morgan, N., Wick A., et al. 2008. Carbon and oxygen levels in Nitinol alloys and the implications for medical device manufacture and durability. In: Berg, M.R.M.B., Proft. J., Proceedings of the International Conference on Shape Memory and Superelastic Technologies, ASM International, Pacific Grove, California, USA, pp. 821–828.
Otsuka, K., Ren, X., 2005. Physical metallurgy of Ti–Ni-based shape memory alloys. Progress in Materials Science 50, 511–678.
Patoor, E., Barbe, P., et al., 1991. Internal stress effect in the shape memory behaviour. Journal de Physique IV C4, C495–C4100.
Pelton, A.R., 2011. Nitinol fatigue: a review of microstructures and mechanisms. Journal of Materials Engineering and Performance 20 (4), 613–617.
Pelton, A.R., DiCello, J., et al., 2000. Optimisation of processing and properties of medical-grade Nitinol wire. Minimally Invasive Therapy & Allied Technologies 9, 107–118.
Pelton, A.R., Duerig, T., et al., 2004. A guide to shape memory and superelasticity in Nitinol medical devices. Minimally Invasive Therapy and Allied Technologies 13 (4), 218–221.
Pelton, A.R., Schroeder, V., et al., 2008. Fatigue and Durability of Nitinol Stents. Journal of Mechanical Behavior of Biomedical Materials 1, 153–164.
Proft, J.L., Melton K.N., et al., 1989. Transformation cycling of Ni–Ti and Ni–Ti–Cu shape memory alloys. In: Doyama, M., Somiya, S., Chang, R.P.H., (Eds.) MRS International Meeting on Advanced Materials, Tokyo, vol. 9 pp. 159–164.
Reedlunn, B., Churchill, C.B., et al., 2012. Tension, compression, and bending of superelastic shape memory alloy tubes. Journal of the Mechanics and Physics of Solidshttp://dxdoi.org/10.1016/j.jmps.2012.12.012.
Reinoehl, M., Bradley, D., Bouthot, R., Proft, J., 2001. The influence of melt practice on final fatigue properties of superelastic NiTi wires. Shape memory and superelastic technologies. In: Russell, S.M., Pelton, A.R., (Eds.), The International Organization on Shape Memory and Superelastic Technologies, Pacific Grove, CA, pp. 397–403.
Robertson, S.W., Pelton, A.R., et al., 2012. Mechanical fatigue and fracture of Nitinol. International Materials Reviews 57 (1), 1–36.
Sawaguchi, T., Kausträter, G., et al., 2003. Crack initiation and propagation in 50.9 at. pct Ni–Ti pseudoelastic shape-memory wires in bending-rotation fatigue. Metallurgical and Materials Transactions A 34 (12), 2847–2860.
Sheriff, J., A. R. Pelton, et al., 2005. Hydrogen effects on Nitinol fatigue. In: Helmus, M., Medlin, D., (Eds.), ASM Materials &

Processes for Medical Devices Conference, ASM, Minneapolis, MN, pp. 38–43.
Smith, K.N., Watson, P., et al., 1970. A stress–strain function for the fatigue of metals. Journal of Materials, JMLSA 5 (4), 767–778.
Smouse, H.B., Nikanorov, A., et al., 2005. Biomechanical forces in the femoropopliteal arterial segment. Endovascular Today, 60–66.
Stebner, A., K. Bhattacharya, 2013. Pasadena, CA.
Stebner, A.P., Brinson, L.C., 2013. Explicit finite element implementation of an improved three dimensional constitutive model for shape memory alloys. Computer Methods in Applied Mechanics and Engineering 257, 17–35.
Stöckel, D., Pelton, A.R., et al., 2004. Self-expanding Nitinol stents: material and design considerations. European Radiology 14, 292–301.
Suresh, S., 1998. Fatigue of Materials. Cambridge University Press, Cambridge, UK.
Thompson, S.A., 2000. An overview of nickel–titanium alloys used in dentistry. International Endodontic Journal 33 (4), 297–310.
Wagner, M.F.-X., Eggeler, G., 2006a. New aspects of bending rotation fatigue in ultra-fine-grained pseudo-elastic NiTi wires. International Journal of Materials Research (formerly Z. Metallkd.) 97 (12), 1687–1696.
Wagner, M.F.X., Eggeler, G., 2006b. Stress and strain states in a pseudoelastic wire subjected to bending rotation. Mechanics of Materials 38 (11), 1012–1025.
Wick, A., X.-Y. Gong, et al., 2005. Bending Fatigue Characteristics of Nitinol. In: Helmus, M., Medlin, D., ASM Materials & Processes for Medical Devices Conference, ASM, Minneapolis, MN, pp. 15–20.
Wick, A., Vöhringer, O., et al., 1995. The Bending Behavior of NiTi. Journal de Physique 5 (IV Coll. C8), 789–794.
Young, J.M., Van Vliet, K.J., 2005. Predicting in vivo failure of pseudoelastic NiTi devices under low cycle, high amplitude fatigue. Journal of Biomedical Materials Research Part B: Applied Biomaterials 72B (1), 17–26.